

PAPER • OPEN ACCESS

## Optimization of experimental parameters for the mechanical characterization of thin elastic films

To cite this article: Wolfgang Gross and Holger Kress 2019 *J. Phys. Commun.* **3** 055021

View the [article online](#) for updates and enhancements.



## PAPER

## Optimization of experimental parameters for the mechanical characterization of thin elastic films

## OPEN ACCESS

## RECEIVED

26 February 2019

## REVISED

6 May 2019

## ACCEPTED FOR PUBLICATION

21 May 2019

## PUBLISHED

3 June 2019

Wolfgang Gross  and Holger Kress

Department of Physics, University of Bayreuth, Bayreuth, Germany

E-mail: [holger.kress@uni-bayreuth.de](mailto:holger.kress@uni-bayreuth.de)**Keywords:** thin films, polyacrylamide, elastic modulus, poisson ratio, rheologySupplementary material for this article is available [online](#)

Original content from this work may be used under the terms of the [Creative Commons Attribution 3.0 licence](#).

Any further distribution of this work must maintain attribution to the author(s) and the title of the work, journal citation and DOI.

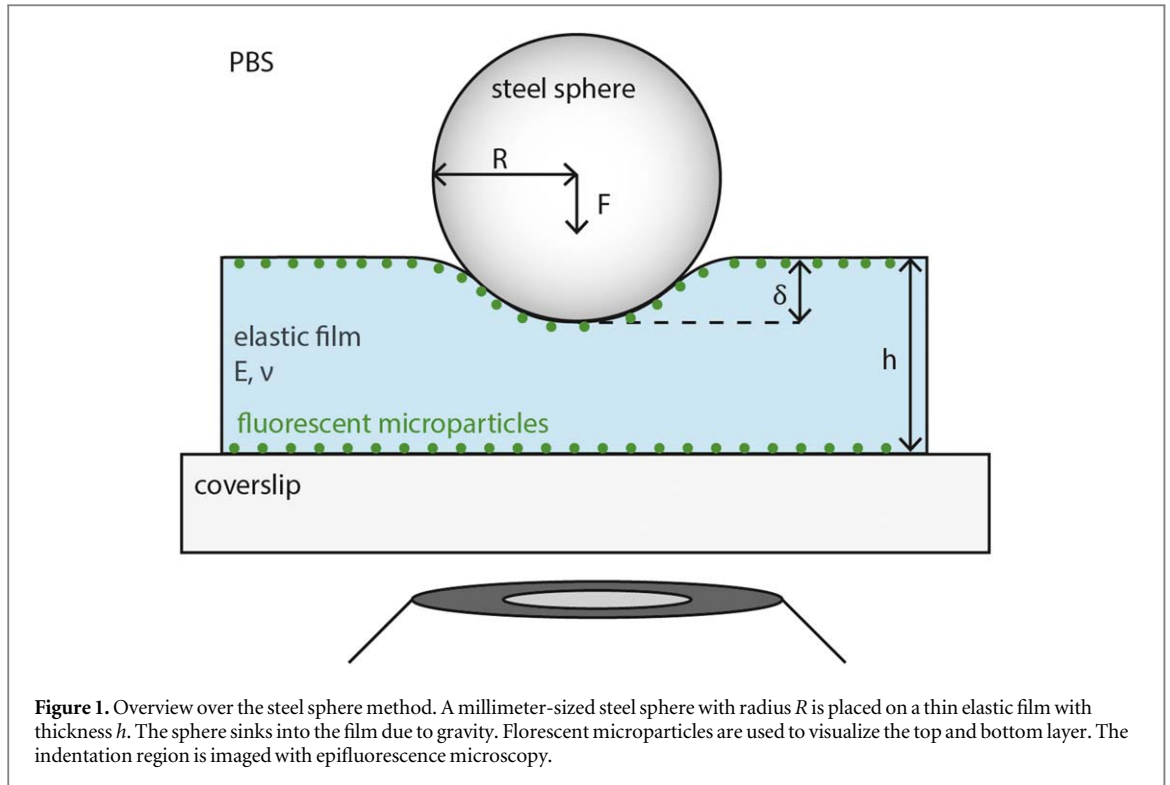
**Abstract**

Indentation experiments are a common tool to measure the elastic properties of many different kinds of samples. However, only few techniques are available to measure the elastic modulus and the Poisson ratio of thin elastic films. Recently, we have described a novel technique based on the steel sphere method to simultaneously measure both parameters of a thin elastic film in a single experiment by placing millimeter-sized steel spheres on the films. In this work, we investigate how various measurement parameters can be tuned to increase the measurement accuracy significantly. These parameters include the number, size, and density of the spheres, the number of data points per sphere and the film thickness. With experiments and simulations we demonstrate that the precision of the measurement can be improved drastically if the parameters are chosen appropriately. We show how to adjust the number of data points to achieve a good balance between workload and accuracy. Additionally, the accuracy can be improved by covering a wide range of different indentation geometries. In particular the use of larger spheres and spheres with a higher density is generally more favorable. We provide Java software to easily adopt the technique and to simplify the data analysis.

**Introduction**

The mechanical interactions between cells and their environment have become a major point of interest in the field of biophysics during the last decades [1]. Cells are able to sense the mechanical stiffness of their environment and in turn alter their behavior depending on the mechanical properties of the environment. Examples include cell proliferation [2], differentiation [3, 4], and cell migration along stiffness gradients [5, 6]. Cells have also been found to be able to exert forces on their environment [7] and various techniques have been developed to quantify these forces. Most notably, traction force microscopy enables spatially and temporally resolved stress measurements of individual cells [8] and has thus become a common tool to study mechanosensitivity [1, 9–11]. Many of these studies rely on a thin, soft film as a simple model system. Materials such as polyacrylamide (PAA) and polydimethylsiloxane (PDMS) are commonly used as a film material due to its tunable mechanical and chemical properties [9, 10].

Multiple techniques to characterize such films are available. On the one hand, tension tests are suitable to characterize macroscopic samples [5]. Indentation experiments on the other hand are a common and well established tool to mechanically characterize thin samples such as polyacrylamide films [9, 12]. Indentation tests are also commonly used to probe the rheological properties of individual cells [13]. For single cell experiments, atomic force microscopy is used in many cases since it provides very detailed control over many experimental parameters [14–16]. For samples with a thickness of at least a few tens of micrometers, the steel sphere method is a suitable technique to characterize the rheological properties. In this technique, small steel spheres with a diameter of about a millimeter are placed on the sample. The spheres sink into the sample due to gravity and the indentation depth can be measured with fluorescent fiducial markers in the top layer of the sample [9, 17, 18].



However, with all those techniques, care has to be taken with regard to finite thickness effects, which can lead to an apparent stiffening when the sample is e.g. placed on a glass coverslip, which is orders of magnitude stiffer than the sample itself [19]. Several models based on linear elastic theory have been developed to account for these finite thickness effects for spherical [12], conical [20] and flat cylindrical indenters [21]. During the last years, finite thickness models accounting for nonlinear material properties have also been developed for spherical and cylindrical indentation geometries [17, 22]. In general, these finite thickness effects can only be neglected when the contact radius of the indenter is significantly smaller than the thickness of the film that is to be probed.

Recently, we have shown that these finite thickness effects are not necessarily a liability but can be exploited to measure the elastic modulus and the Poisson ratio of a thin film simultaneously with the steel sphere method [18]. In this work, we show how the accuracy of the technique can be improved drastically by a good choice of measurement parameters such as the number and size of the spheres or the film thickness. Even though the technique is commonly referred to as the steel sphere method, other materials with different densities such as gold can also be used.

## Theory

Our technique is based on a theoretical model developed by Dimitriadis *et al* which accounts for finite thickness effects [12]. An overview of the method is shown in figure 1. A sphere with radius  $R$  indents a soft film with elastic modulus  $E$  and Poisson ratio  $\nu$ . The model assumes that the film is a homogeneous and isotropic elastic material, which is probed within the linear regime. Additionally, adhesion effects are assumed to be negligible during indentation. The sphere and the film are completely immersed in a fluid, e.g. PBS. The sphere is pushed into the film with an indentation force  $F$  resulting in an indentation depth  $\delta$ . In our case, the indentation force is given by gravity:

$$F = \frac{4}{3}R^3\pi g(\rho_s - \rho_{PBS}). \quad (1)$$

$g$  denotes the gravitational acceleration,  $\rho_s$  the density of the spheres and  $\rho_{PBS}$  the density of the surrounding medium. For a film of thickness  $h$ , the elastic modulus is given by [12]

$$E = \frac{3(1 - \nu^2)F}{4(R\delta^3)^{0.5}C} \quad (2)$$

with

$$C = 1 - \frac{2\alpha_0}{\pi}\chi + \frac{4\alpha_0^2}{\pi^2}\chi^2 - \frac{8}{\pi^3}\left(\alpha_0^3 + \frac{4\pi^2}{15}\beta_0\right)\chi^3 + \frac{16\alpha_0}{\pi^4}\left(\alpha_0^3 + \frac{3\pi^2}{5}\beta_0\right)\chi^4 \quad (3)$$

and the parameters  $\alpha_0$  and  $\beta_0$ , which are functions of the film's Poisson ratio. In the case of a film bonded to a stiff surface  $\alpha_0$  and  $\beta_0$  are given by [12]:

$$\alpha_0 = -\frac{1.2876 - 1.4678\nu + 1.3442\nu^2}{1 - \nu}, \quad (4)$$

$$\beta_0 = \frac{0.6387 - 1.0277\nu + 1.5164\nu^2}{1 - \nu}. \quad (5)$$

$\chi = \sqrt{R\delta}/h$  is a function of the indentation geometry. The theory is valid in the range  $0 \leq \chi \leq 1$  and represents an *ab initio* extension of the Hertzian solution which is valid for an infinite half space [23].

Using the Hertzian model, which is recovered in the case of  $\chi = 0$ , it is only possible to measure the term  $E/(1 - \nu^2)$ . However, as we have recently demonstrated experimentally [18], both elastic parameters can be recovered when finite thickness effects are exploited. Since the correction term  $C$  depends on the Poisson ratio and the indentation geometry, both parameters can be determined reliably by fitting equation (1) to indentation data  $\delta(h, R)$ .

## Materials and methods

### Sample preparation

Polyacrylamide and Poly-N-isopropylacrylamide films were prepared as described [18] in analogy to a previously published protocol [5, 24]. Briefly,  $40 \times 22 \text{ mm}^2$  sized coverslips (Glaswarenfabrik Karl Hecht, Sondheim v. d. Röhn, Germany) were cleaned and coated with (3-aminopropyl)trimethoxysilane (Sigma-Aldrich, St. Louis, MO) and aqueous 0.5% glutaraldehyde solution (Sigma-Aldrich) to covalently bind the coverslips to the films. A second coverslip with a diameter of 15 mm (Menzel-Gläser, Braunschweig, Germany) was coated hydrophobically with RainX (Krako Car Care International) according to the manufacturers' protocol to facilitate better detachment of the films [25].

To polymerize a thin polyacrylamide film, a monomer solution containing 10% w/v acrylamide (AA, Sigma-Aldrich) and 0.06% w/v N,N'-methylenebisacrylamide (BIS) in phosphate buffered saline ( $1 \times$  PBS,  $0.2 \text{ g l}^{-1}$  KCl,  $8.0 \text{ g l}^{-1}$  NaCl,  $1.44 \text{ g l}^{-1}$   $\text{Na}_2\text{HPO}_4$ ,  $0.24 \text{ g l}^{-1}$   $\text{KH}_2\text{PO}_4$  in deionized water) was prepared. As a catalyst, we added 1/2000 v/v N,N,N',N'-Tetramethylethylenediamine (TEMED, Thermo Fisher Scientific, Waltham, MA). Furthermore, we added fluorescent microparticles (FluoSpheres, diameter  $0.2 \mu\text{m}$ , Ex/Em: 505/515 nm, carboxylated surface modification, Thermo Fisher Scientific) which diffuse to the top and bottom layer of the films during the polymerization, serving as a marker for both layers. The polymerization reaction was started by adding 1/200 v/v freshly prepared 10% w/v aqueous ammonium-persulfate (APS) solution.

A thin film of Poly-N-Isopropylacrylamide (PNIPA) was prepared similarly. A monomer solution containing 10% w/v N-isopropylacrylamide (NIPA, Sigma-Aldrich) and 0.1% w/v BIS was used. Since we found that NIPA solutions polymerized slower than the PAA solution, we degassed it for 45 min and doubled both the TEMED concentration to 1/1000 v/v and the APS concentration to 1/100 v/v.

To prepare thin films,  $15 \mu\text{l}$  of the monomer solutions were placed between one RainX- and one glutaraldehyde-coated coverslip and polymerized at room temperature and at an air humidity of 60%–80% to minimize evaporation effects.

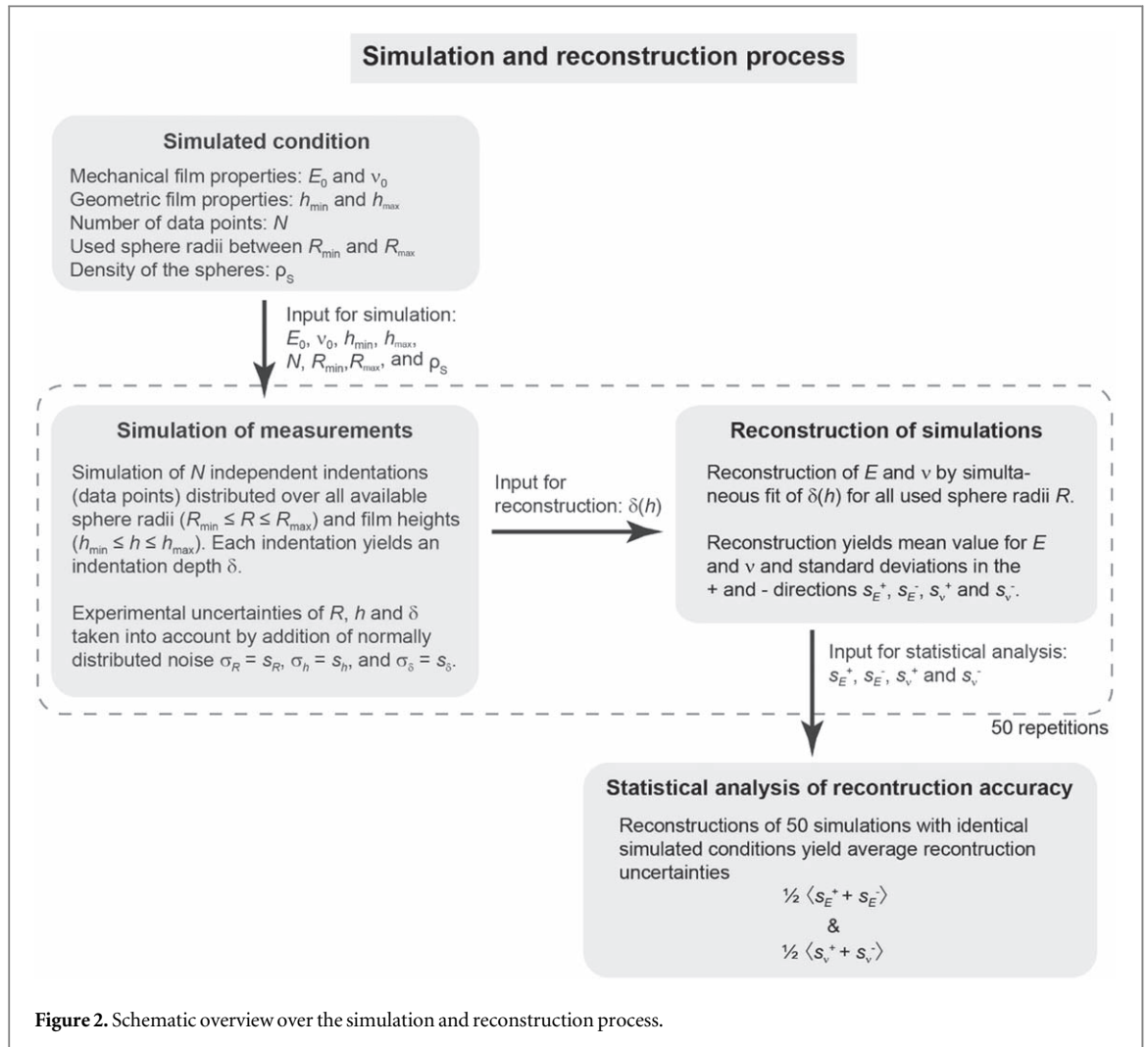
### Measurement setup, imaging and data analysis

Indentation experiments were carried out as described before [18]. The films were soaked in  $1 \times$  PBS, mounted on an inverted, motorized epifluorescence microscope (Nikon Ti-E, Nikon, Tokyo, Japan) and steel (AISI 420C, density  $\rho_s = (7.76 \pm 0.15) \text{ g cm}^{-3}$ ) spheres (grade 10, IHSD-Klarmann, Bamberg, Germany) with nominal radii  $R$  between  $200 \mu\text{m}$  and  $500 \mu\text{m}$  were placed on the film. An overview over all spheres used for this study is given in table 1. Experiments with PAA were carried out at room temperature while all measurements with PNIPA were performed at  $30 \text{ }^\circ\text{C}$  which is slightly below the lower critical solution temperature of  $32 \text{ }^\circ\text{C}$  for our system.

Fluorescence images of the indentation region were acquired using  $40\times$  (CFI Apo LWD  $40\times$  WI  $\lambda\text{S}$ , numerical aperture 1.15, Nikon) and  $60\times$  (CFI Plan Apo IR  $60\times$  WI, numerical aperture 1.27, Nikon) water immersion objectives in combination with a 14 bit EMCCD camera (Andor Luca R, Andor Technology, Belfast, Northern Ireland). We acquired axial image stacks of the indentation region with a vertical image to image distance of  $0.2 \mu\text{m}$  which is sufficient to oversample the image given the axial resolution of the microscope [26].

**Table 1.** Indentation forces of all the spheres used in the experiments and simulations.

Radius $R/\mu\text{m}$	Indentation force $F/\mu\text{N}$	
	Steel	Gold
200	2.2	6.0
250	4.3	11.7
350	11.9	32.2
400	17.8	48.1
500	34.8	94.0



After the measurement the sphere was moved with a small magnet to acquire multiple data points at different locations. The indentation depth  $\delta$  was determined from the stacks as described [18].

### Simulation of indentation data and reconstruction of the elastic parameters

The simulations of indentation data were carried out as described in figure 2. In the following, the term ‘condition’ summarizes the values of the true elastic modulus  $E_0$ , the true Poisson ratio  $\nu_0$ , the thickness range of the film  $h_{\min} - h_{\max}$ , the number of data points per measurement  $N$ , and the used spheres with radii  $R$  and with a density  $\rho_s$ . For every condition we simulated 50 individual measurements. Every measurement consists of  $N$  independent data points, each of which represents the indentation of a steel sphere with a given radius  $R$  into the film at one particular film height. If not stated otherwise, the density of the spheres was kept constant at the density of steel (AISI 420C,  $\rho_s = (7.76 \pm 0.15) \text{ g cm}^{-3}$ ). For some conditions we also tested gold spheres which

have a higher density of  $\rho_S = 19.3 \text{ g cm}^{-3}$  [27]. The total number of data points  $N$  was split up evenly over all the spheres used. For every data point, we randomly chose a film thickness between  $h_{\min}$  and  $h_{\max}$  and solved equation (2) numerically for the indentation depth  $\delta$ . In order to account for the measurement errors, we randomized  $R$ ,  $\delta$ , and  $h$  by adding a normally distributed offset with a standard deviation  $\sigma_R$ ,  $\sigma_\delta$  and  $\sigma_h$  of our experimental uncertainties  $s_R = 1.5 \text{ }\mu\text{m}$ ,  $s_\delta = 0.2 \text{ }\mu\text{m}$ , and  $s_h = 1.5 \text{ }\mu\text{m}$  if not stated otherwise.

We applied the previously developed least squares fitting algorithm [18] to reconstruct the elastic parameters and their respective errors from the indentation data. To calculate the errors of the elastic parameters in one measurement, we used a Monte Carlo approach [28]. In 1000 replications, the indentation depth, the sphere radius and the gel height were randomized by normally distributed offsets with a standard deviation of the experimental uncertainties given above. Then we fitted equation (2) to the indentation data  $\delta(h, R)$  for all replications to determine the probability distributions of  $E$  and  $\nu$ . As described [18], the probability distributions were then fitted with asymmetric Gaussian distributions in Matlab (The Mathworks, Inc., Natic, MA) to determine  $E_{-s_E}^{+s_E}$  and the Poisson ratio  $\nu_{-s_\nu}^{+s_\nu}$ , the elastic modulus and their respective uncertainties of a single measurement. If any of the fits failed per condition, i.e. in any of the 50 simulated measurements, we considered the whole condition not to be reconstructable.

Then, we averaged the reconstruction uncertainties over all 50 measurements and report the mean reconstruction uncertainties  $\langle s_E \rangle = \langle s_E^+ + s_E^- \rangle / 2$  and  $\langle s_\nu \rangle = \langle s_\nu^+ + s_\nu^- \rangle / 2$  as a measure of how precisely the elastic parameters can be determined in a particular condition. In all tested conditions, we were able to reconstruct the ground truth values within the margin of error if not stated otherwise. The Java source code of the software used to do the calculations is available in the SI.

## Results

### Choice of data point count and film thickness

We investigated how precisely our simulated data can predict the reconstruction uncertainties  $\langle s_E \rangle$  and  $\langle s_\nu \rangle$  resulting from experimental data. For this purpose, 60 measured data points acquired on a polyacrylamide film (10% AA, 0.03% BIS,  $E_0 = 15.1_{-1.5}^{+1.2}$  kPa,  $\nu_0 = 0.48 \pm 0.02$ ,  $h = (55 - 120) \text{ }\mu\text{m}$ ) and 50 measured data points on poly-N-isopropylacrylamide (PNIPA, 10% NIPA, 0.1% BIS,  $E_0 = (11.7 \pm 0.7)$  kPa,  $\nu_0 = 0.33_{-0.11}^{+0.05}$ ,  $h \approx 90 \text{ }\mu\text{m}$ ) were split up into smaller, yet independent data sets and reconstructed independently. The data points were acquired with spheres of  $R = 200, 250, 350, 400,$  and  $500 \text{ }\mu\text{m}$  on the PAA film and  $R = 200$  and  $400 \text{ }\mu\text{m}$  on the PNIPA film. The experimental uncertainties of the indentation were  $s_\delta = 0.3 \text{ }\mu\text{m}$  for spheres with  $R \leq 350 \text{ }\mu\text{m}$  and  $s_\delta = 0.4 \text{ }\mu\text{m}$  for spheres with  $R \geq 400 \text{ }\mu\text{m}$ . Using the same conditions, we simulated indentation data as described in the materials and methods section.

The average measurement uncertainties are shown in figure 3 as a function of the number of independent data points  $N$  used per reconstruction. The measurement uncertainties decreased in all of these cases with increasing number of measurement points and are well described by the heuristic fit function

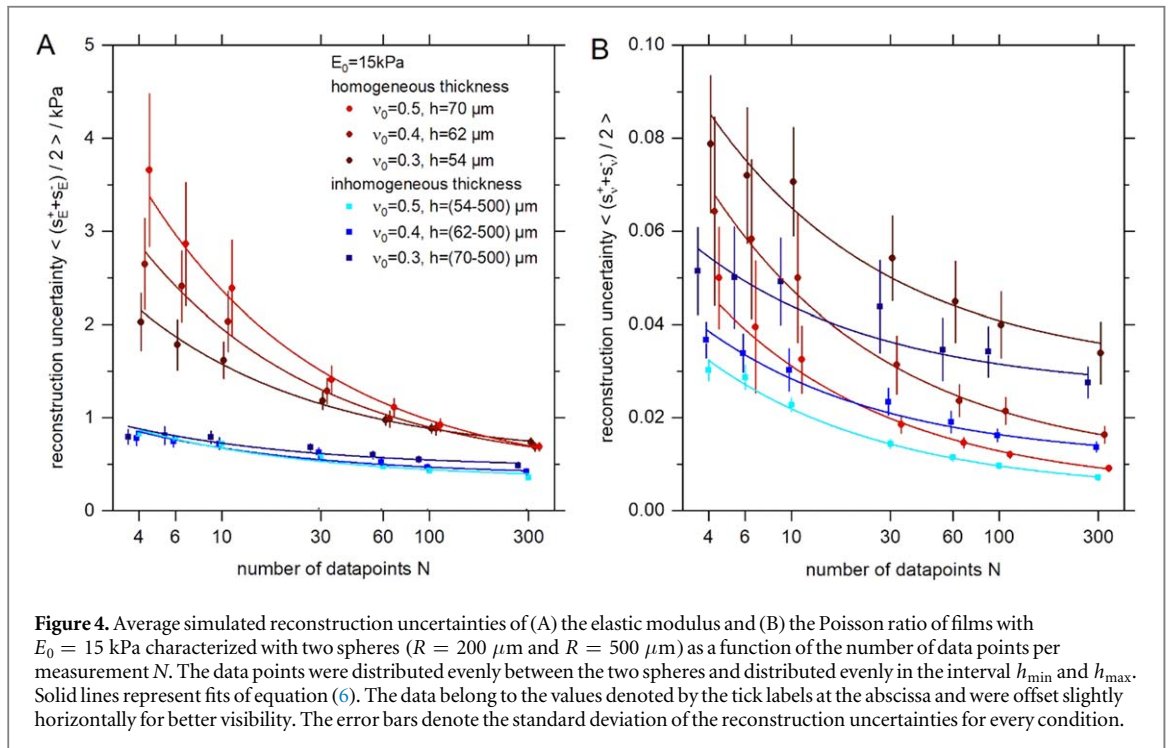
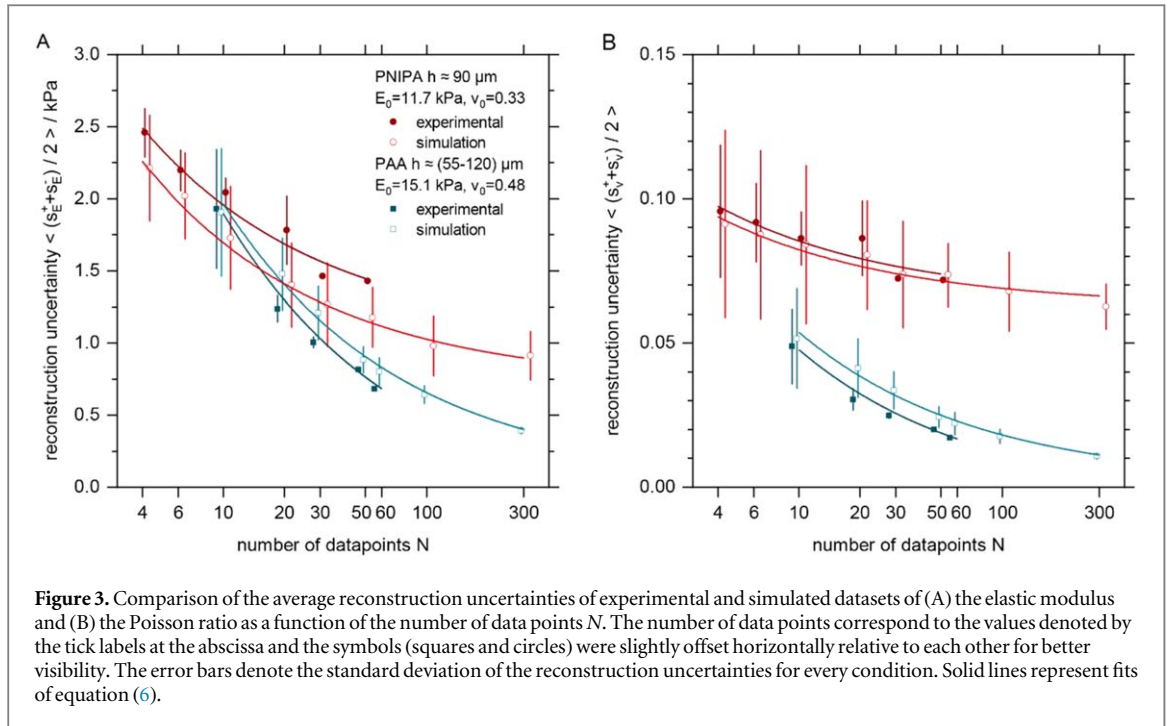
$$\langle s_{E,\nu} \rangle = A_{E,\nu} + \frac{B_{E,\nu}}{\sqrt{N}} \quad (6)$$

For both film types, the uncertainties from simulated and measured datasets and their dependence on the number of data points per reconstruction were in excellent agreement. Therefore, we conclude that our approach for the simulation of the uncertainties is suitable to predict the accuracy of real measurements.

We further investigated how the number of measurement points  $N$  influences the measurement accuracy by simulating the indentation of two spheres with radii of  $200 \text{ }\mu\text{m}$  and  $500 \text{ }\mu\text{m}$  into films with an elastic modulus of  $E_0 = 15 \text{ kPa}$  and various Poisson ratios of  $\nu = 0.3, 0.4,$  and  $0.5$ . Furthermore, we investigated two different film geometries.

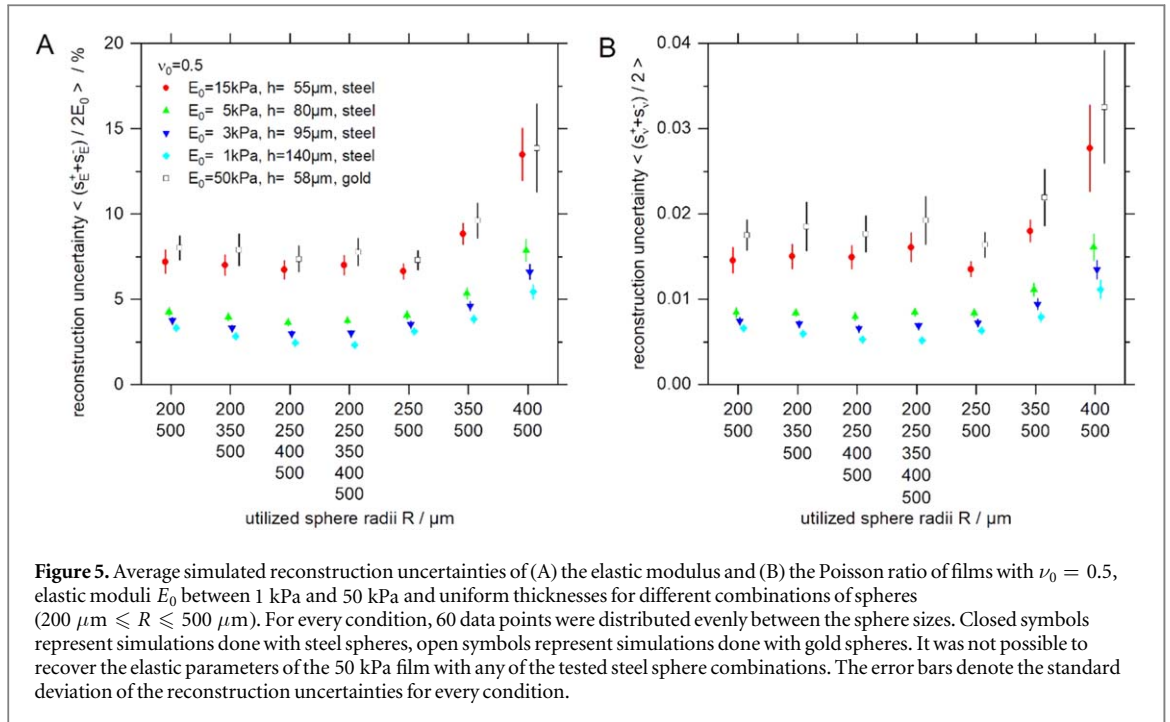
The first geometry includes films which have a uniform thickness  $h$ . For our simulations, we chose  $h$  such that the total range of  $\chi$  values covered by both spheres is maximal, therefore providing optimal contrast for the reconstruction of  $E$  and  $\nu$ . This is the case when the indentation geometry of the largest sphere corresponds to  $\chi(R = 500 \text{ }\mu\text{m}, h, \delta(h)) = 1$ . For example in the case of the incompressible film with a thickness of  $h = 54 \text{ }\mu\text{m}$ , the sphere with  $R = 200 \text{ }\mu\text{m}$  is expected to sink in  $2.5 \text{ }\mu\text{m}$  which corresponds to  $\chi = 0.39$  while the sphere with  $R = 500 \text{ }\mu\text{m}$  is expected to sink in  $6.8 \text{ }\mu\text{m}$  which corresponds to  $\chi = 1$  (see supplementary information (SI) figure 1(A) is available online at [stacks.iop.org/JPCO/3/055021/mmedia](https://stacks.iop.org/JPCO/3/055021/mmedia)). Thicknesses lower than  $h$  would correspond to  $\chi > 1$  for which equation (3) is not valid [12]. A thicker film would decrease the contrast in the correction factor achievable by both spheres.

The second geometry consists of films with a thickness that varies between  $h_{\min}$  and  $h_{\max} = 500 \text{ }\mu\text{m}$ . We chose  $h_{\min}$  such that  $\chi(R = 500 \text{ }\mu\text{m}, h_{\min}, \delta(h_{\min})) = 1$ . At a thickness of  $500 \text{ }\mu\text{m}$ , the values of  $\chi$  are below 0.2 for both spheres in all conditions. In this case, the correction factor  $C$  varies only slightly as a function of  $\nu$  (see SI figure 2 and Gross and Kress [18]). Therefore, we consider the small differences in contrast between the



different conditions to be negligible. Under all conditions, the  $N$  data points were chosen equally spaced between  $h_{\min}$  and  $h_{\max}$ . The resulting probability distributions of  $\chi$  covered by both spheres in the case of  $\nu_0 = 0.5$  are shown in SI figure 1(B).

The resulting reconstruction uncertainties of the elastic modulus and the Poisson ratio are shown in figure 4. In general, it can be stated that the higher the Poisson ratio, the more accurately it can be determined (figure 4(B)). Interestingly, this is different for the elastic modulus. Our results for films with a uniform thickness show that the reconstruction of the elastic modulus is more accurate at low Poisson ratios (figure 4(A), circles). As it was the case for the experimental data, the reconstruction uncertainty decreases in all conditions with increasing number of measurement points (figure 4, both panels) and is well described by equation (6) (the fit parameters  $A$  and  $B$  were positive in all cases). Therefore, by increasing the number of data points, the uncertainties can at most be reduced by the factor  $B/(A + B)$  and every increase in the number of data points



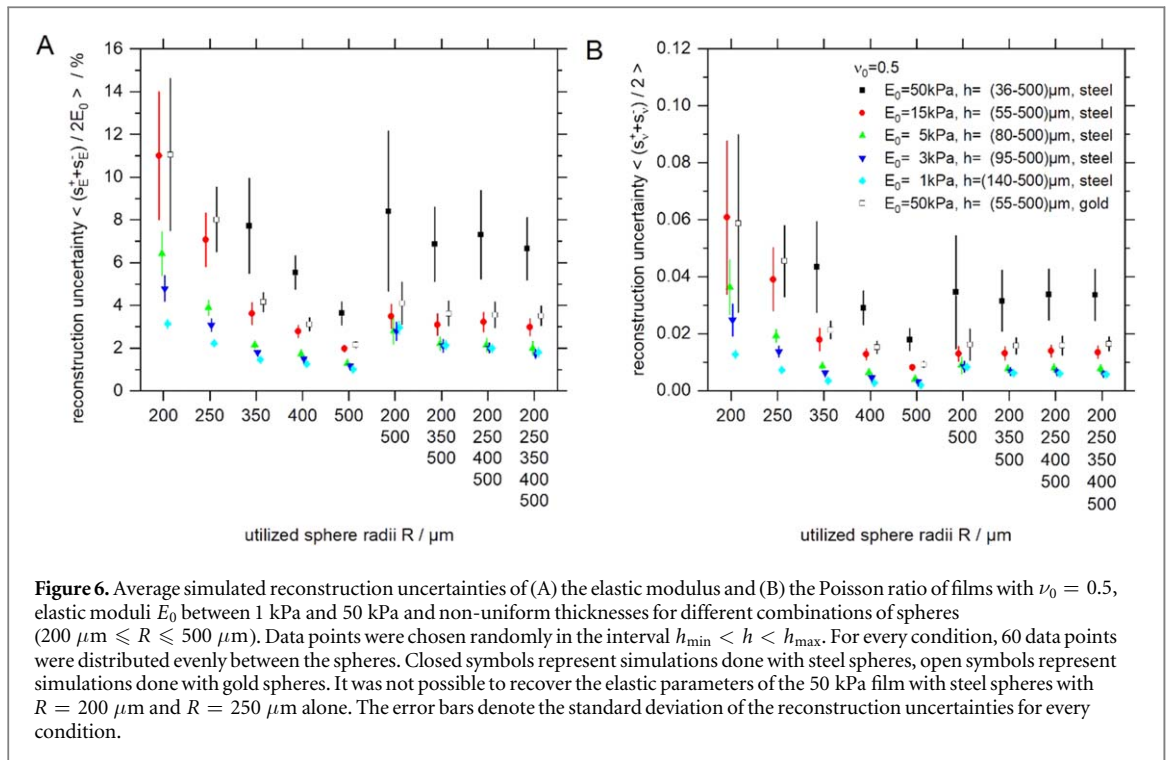
yields diminishing returns. For our parameter set,  $N = 60$  appears to be a good compromise between the overall reconstruction accuracy and the workload required for data acquisition and evaluation. At this point, the remaining uncertainty  $A + 0.13B$  is of the same order of magnitude as  $A$  and thus, any increase in  $N$  only yields a marginal improvement. Notably, the reconstruction uncertainty of the elastic modulus is barely influenced by the Poisson ratio when a film with non-uniform thickness is used (figure 4(A) squares). In this case, the reconstruction accuracy is also barely influenced by the number of data points per measurement. Therefore, only a few data points ( $N < 60$ ) are required to determine the elastic modulus.

### Choice of sphere count, radii, and density

The choice of the sphere radii also has a major influence on the reconstruction accuracy. In theory, the upper limit for the sphere radius is given by the theoretical geometric limitation that  $\sqrt{R \delta} \leq h$ . Due to gravity a larger sphere will sink deeper into the film which results in an upper limit for the sphere radius given by  $R_{\text{max}} = h^2 / \delta$ . On the other hand, a sphere that is too small does not sink in enough such that the indentation depth is below the resolution limit of the set-up. Based on these limitations, we chose to investigate the use of up to 5 spheres with radii between  $200 \mu\text{m}$  and  $500 \mu\text{m}$  and chose the film thickness such that  $\chi \approx 1$  for  $R = 500 \mu\text{m}$  in the thinnest region of the film. We varied the elastic modulus between 1 and 50 kPa and investigated two Poisson ratios of  $\nu = 0.3$  and  $0.5$ . We kept the total number of data points constant at  $N = 60$  and distributed them evenly over all sphere sizes.

There are two major cases that need to be distinguished. When a film with a homogeneous thickness is used, the reconstruction is not possible with only one sphere since the correction term  $C$  is identical for all data points (see equation (3)). Therefore, the use of at least two spheres is mandatory in this case. The reconstruction accuracies strongly depend on the size of the spheres that are used, both for incompressible films (figure 5) and films with  $\nu = 0.3$  (SI figure 3). In all tested conditions, the combination of 5 different spheres yielded one of the most precise results. The use of only two relatively large spheres with radii of  $400 \mu\text{m}$  and  $500 \mu\text{m}$  was least precise. In SI figure 4(A), it can be seen that in this case, only a very limited range of  $0.8 \leq \chi \leq 1$  is covered.

The situation is very different when a film with an inhomogeneous thickness is available. When data points at different film heights are acquired, one sphere can cover a wide range of  $\chi$  values (see SI figure 4(B)). Therefore, the reconstruction is also possible with only one sphere. Our simulation shows that the reconstruction is most precise when only one sphere and in particular, the largest sphere suitable for a film with  $\nu_0 = 0.5$  (figure 6) and  $\nu_0 = 0.3$  (SI figure 5) is used. We attribute this to the fact that in this case, a large range of  $\chi$  values can be covered by one sphere. For this reason, there is no need to utilize smaller spheres which, in general, offer less resolution since the relative error of the indentation is larger. Additionally, small spheres cover a smaller range of lower  $\chi$  values where the contrast factor  $C$  depends only slightly on the Poisson ratio (see SI figure 2).



Notably, the reconstruction is generally more precise on soft films (see figures 5, 6 and SI figures 3 and 5). We attribute this to the fact that the relative error of the indentation is lower on softer films since the spheres sink in deeper. For example, in the case of  $E_0 = 50 \text{ kPa}$  and  $\nu_0 = 0.5$ , the steel sphere with a radius of  $R = 200 \mu\text{m}$  is only expected to sink approximately  $1.2 \mu\text{m}$  into a film with a thickness of  $55 \mu\text{m}$ , thus the error of the indentation about 17%. For this reason, the reconstruction was not possible with any of the tested steel sphere combinations on a homogeneous film. One way to alleviate this issue is to increase the indentation depth by placing spheres with a higher density on the film. When gold spheres with a density of  $\rho_S = 19.3 \text{ g cm}^{-3}$  are used on a slightly thicker film ( $h = 55 \mu\text{m}$ ) the indentation depth of a sphere with  $R = 200 \mu\text{m}$  increases to  $2.5 \mu\text{m}$ . As a consequence, the reconstruction was possible in all cases and the uncertainties are comparable to the conditions when steel spheres were used on a 15 kPa gel. This can be understood from equation (2). Since the fraction  $E/(\rho_S - \rho_{\text{PBS}})$  is similar in both cases, the relative reconstruction uncertainty of the elastic modulus and the reconstruction uncertainty of the Poisson ratio are also similar.

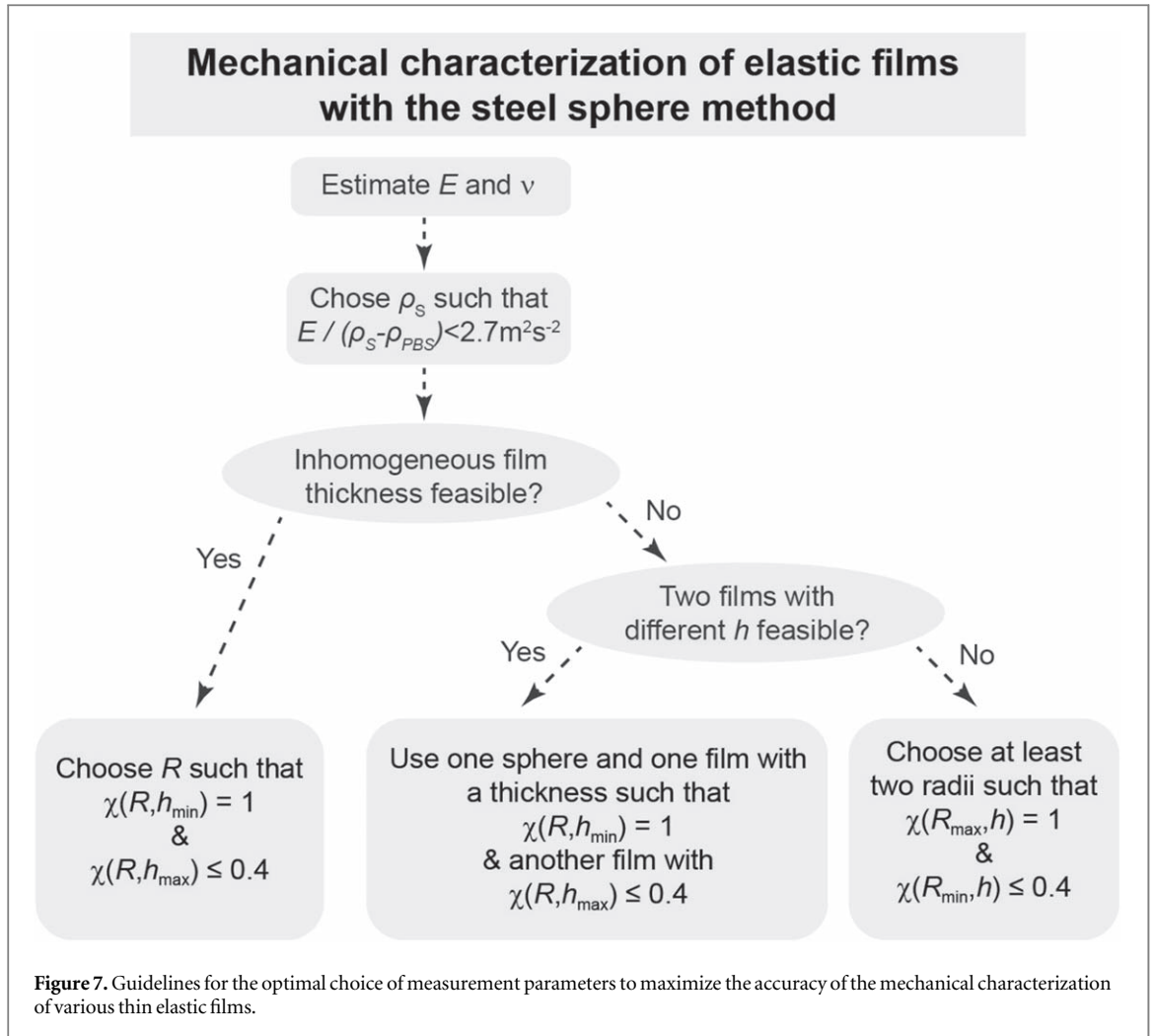
## Discussion

By simulating the indentation of metal spheres into thin films we are able to reproduce our experimental uncertainties of the elastic modulus and the Poisson ratio. Thus, our simulation approach is suitable to predict the precision of real experiments. Our results suggest that there are three general points that should be considered during the planning of such experiments. First of all, we have shown that an increase in the number of data points does not necessarily make the reconstruction significantly more accurate. For our set-up, measuring more than 60 individual data points only results in marginal improvements. Secondly, our simulations demonstrate that the use of larger spheres generally leads to more accurate results. Thirdly, it is highly beneficial to cover a wide range of  $\chi$  values during the experiment. In particular, it is most important to cover the range between  $\chi = 0.4$  and the highest possible value  $\chi = 1$ . Guidelines for the optimal choice of measurement parameters for a given set of boundary conditions of the samples are summarized in figure 7.

To calculate the indentation depth and  $\chi$  during the planning phase, a rough estimate of the elastic parameters of the film are necessary. We suggest running first preliminary experiments to get a rough estimate for the elastic modulus and, if available, estimate the Poisson ratio using literature data.

With fixed elastic properties, we have investigated three basic ways to achieve a broad range of different geometries and thus,  $\chi$  values. One can either use different sphere densities, sphere radii or a film with an inhomogeneous thickness.

The density of the spheres should be chosen such that the indentations of the smallest sphere can be easily resolved. We were able to reconstruct the elastic properties in all tested conditions when the fraction



$E/(\rho_S - \rho_{PBS})$  was smaller than  $2.7 \text{ m}^2 \text{ s}^{-2}$ . However, the reconstruction was significantly more precise in conditions where  $E/(\rho_S - \rho_{PBS})$  was one order of magnitude smaller.

Our results suggest that films with a non-uniform thickness offer great benefits. On the one hand, the accuracy of the reconstruction is vastly superior. In comparison to films with a homogeneous thickness the uncertainty of the Poisson ratio can be reduced significantly by up to 40% and the uncertainty of the elastic modulus can be reduced by up to 75%. On the other hand, films with an inhomogeneous thickness enable the reconstruction with only one sphere size, which reduces the experimental complexity. In fact, the reconstruction of the elastic parameters of such films is most precise when only one large sphere is used.

However, a film with a very wide thickness distribution might be unfeasible in an actual experiment due to the slope of the upper surface. A practical solution could be to choose  $h_{\max}$  such that  $\chi(R, h_{\max}, \delta(h_{\max})) \approx 0.4$  to cover the range from  $\chi = 0.4$  to 1. Another possible solution to this problem would be to use two films with different thicknesses but otherwise identical properties. When only a film with a homogeneous thickness is available, the only option to reconstruct both elastic parameters is to choose a set of different sphere radii. In this case, we suggest a large sphere to cover the point  $\chi = 1$  in combination with a smaller sphere to cover the lower  $\chi$ -range. The indentations of the small sphere however should be large enough so that they can be easily resolved. The use of more than two spheres yielded only marginal improvements.

Additionally, we would like to highlight the fact that multiple radii offer another benefit. Since equation (2) is highly nonlinear in  $R$ , multiple radii can be used to test whether equation (2) is valid for the indentation data. Since the indentation depths and contact areas significantly depend on the radii of the spheres, multiple spheres with different radii offer the possibility to test that the film is probed within the linear elastic regime or whether for example adhesion effects between the film and the indenter are at play. In this case, these effects have to be accounted for by other models [17, 29–31].

## Conclusions

The steel sphere method is a common tool to probe the stiffness of soft, thin films with a stiffness in the range of mammalian tissue [9, 29, 32]. Recently, we have extended the method such that not only the elastic modulus but also the Poisson ratio can be measured [18]. In this work, we have demonstrated that the reconstruction accuracy of the elastic modulus and the Poisson ratio can be determined with a statistical approach. We have shown that the gel geometry and the radii and density of the spheres that are used have a major impact on the reconstruction accuracy. To maximize this accuracy, we suggest to carefully plan mechanical characterization experiments according to the guidelines given in this manuscript.

As a rule of thumb, the density of the spheres should be chosen such that the fraction  $E/(\rho_s - \rho_{\text{PBS}})$  is less than  $2.7 \text{ m}^2 \text{ s}^{-2}$ . The contact geometry can then be adjusted by the choice of the sample thickness and the sphere radii and should be chosen such that  $0.4 \leq \chi \leq 1$ . A film with an inhomogeneous thickness should be used for the measurement whenever possible. In this case, the sample can be probed with one sphere radius and the measurement is generally more accurate than the characterization of a film with a homogeneous thickness where two sphere radii should be used.

## Acknowledgments

We would like to acknowledge support from the DFG (INST 91/289-1 FUGG), the German Academic Scholarship Foundation (Studienstiftung des deutschen Volkes), the University of Bayreuth Graduate School and the Elite Network of Bavaria (ENB). This publication was funded by the German Research Foundation (DFG) and the University of Bayreuth in the funding program Open Access Publishing.

## Conflicts of interest

There are no conflicts of interest to declare.

## Author contributions

H Kress and W Gross designed the research. W Gross performed the research and analyzed the data. Both authors discussed the results and wrote the manuscript.

## ORCID iDs

Wolfgang Gross  <https://orcid.org/0000-0002-6064-9878>

## References

- [1] Chen C S 2008 Mechanotransduction—a field pulling together? *J. Cell Sci.* **121** 3285–92
- [2] Leach J B, Brown X Q, Jacot J G, DiMilla P A and Wong J Y 2007 Neurite outgrowth and branching of PC12 cells on very soft substrates sharply decreases below a threshold of substrate rigidity *J. Neural Eng.* **4** 26–34
- [3] Engler A J, Rehfeldt F, Sen S and Discher D E 2007 Mirotoissue elasticity: measurements by atomic force microscopy and its influence on cell differentiation *Method. Cell Biol.* **83** 521–45
- [4] Lanniel M, Huq E, Allen S, Buttery L, Williams P M and Alexander M R 2011 Substrate induced differentiation of human mesenchymal stem cells on hydrogels with modified surface chemistry and controlled modulus *Soft Matter* **7** 6501–14
- [5] Pelham R J Jr and Wang Y 1997 Cell locomotion and focal adhesions are regulated by substrate flexibility *Proc. Natl Acad. Sci. USA* **94** 13661–5
- [6] Lo C M, Wang H B, Dembo M and Wang Y L 2000 Cell movement is guided by the rigidity of the substrate *Biophys. J.* **79** 144–52
- [7] Harris A K, Wild P and Stopak D 1980 Silicone rubber substrata: a new wrinkle in the study of cell locomotion *Science* **208** 177–9
- [8] Dembo M and Wang Y L 1999 Stresses at the cell-to-substrate interface during locomotion of fibroblasts *Biophys. J.* **76** 2307–16
- [9] Kraning-Rush C M, Carey S P, Califano J P and Reinhart-King C A 2012 Quantifying traction stresses in adherent cells *Methods Cell. Biol.* **110** 139–78
- [10] Style R W, Boltyskiy R, German G K, Hyland C, MacMinn C W, Mertz A F, Wilen L A, Xu Y and Dufresne E R 2014 Traction force microscopy in physics and biology *Soft Matter* **10** 4047–55
- [11] Kurzawa L, Vianay B, Senger F, Vignaud T, Blanchoin L and Thery M 2017 Dissipation of contractile forces: the missing piece in cell mechanics *Mol. Biol. Cell* **28** 1825–32
- [12] Dimitriadis E K, Horkay F, Maresca J, Kachar B and Chadwick R S 2002 Determination of elastic moduli of thin layers of soft material using the atomic force microscope *Biophys. J.* **82** 2798–810
- [13] Petersen N O, McConnaughey W B and Elson E L 1982 Dependence of locally measured cellular deformability on position on the cell, temperature, and cytochalasin-B *P. Natl. Acad. Sci.-Biol.* **79** 5327–31
- [14] Radmacher M 2002 Measuring the elastic properties of living cells by the atomic force microscope *Method. Cell Biol.* **68** 67–90

- [15] Rianna C, Ventre M, Cavalli S, Radmacher M and Netti P A 2015 Micropatterned azopolymer surfaces modulate cell mechanics and cytoskeleton structure *ACS Appl. Mater. Inter.* **7** 21503–10
- [16] Kollmannsberger P and Fabry B 2011 Linear and nonlinear rheology of living cells *Annu. Rev. Mater. Res.* **41** 75–97
- [17] Long R, Hall M S, Wu M M and Hui C Y 2011 Effects of gel thickness on microscopic indentation measurements of gel modulus *Biophys. J.* **101** 643–50
- [18] Gross W and Kress H 2017 Simultaneous measurement of the Young's modulus and the Poisson ratio of thin elastic layers *Soft Matter* **13** 1048–55
- [19] Domke J and Radmacher M 1998 Measuring the elastic properties of thin polymer films with the atomic force microscope *Langmuir* **14** 3320–5
- [20] Santos J A C, Rebelo L M, Araujo A C, Barros E B and de Sousa J S 2012 Thickness-corrected model for nanoindentation of thin films with conical indenters *Soft Matter* **8** 4441–8
- [21] Cao Y P, Ma D C and Raabe D 2009 The use of flat punch indentation to determine the viscoelastic properties in the time and frequency domains of a soft layer bonded to a rigid substrate *Acta Biomater.* **5** 240–8
- [22] Fessel A and Dobreiner H G 2018 Nonlinear compliance of elastic layers to indentation *Biomech. Model. Mechanobiol.* **17** 419–38
- [23] Hertz H R 1882 Ueber die Beruehrung elastischer Koerper *J. Reine Angew. Math.* **92** 156–71
- [24] Aplin J D and Hughes R C 1981 Protein-derivatised glass coverslips for the study of cell-to substratum adhesion *Anal. Biochem.* **113** 144–8
- [25] Plotnikov S V, Sabass B, Schwarz U S and Waterman C M 2014 High-resolution traction force microscopy *Methods Cell. Biol.* **123** 367–94
- [26] Jonkman J E, Swoger J, Kress H, Rohrbach A and Stelzer E H 2003 Resolution in optical microscopy *Methods Enzymol.* **360** 416–46
- [27] Weast R C and Astle M J 1980 *CRC Handbook of Chemistry and Physics* 61 edn (Boca Raton, Florida: CRC Press Inc.)
- [28] Press W H, Teukolsky S A, Vetterling W T and Flannery B P 2007 *Numerical Recipes: The Art of Scientific Computing* (Cambridge: Cambridge University Press) 3
- [29] Hall M S, Long R, Hui C Y and Wu M M 2012 Mapping three-dimensional stress and strain fields within a soft hydrogel using a fluorescence microscope *Biophys. J.* **102** 2241–50
- [30] Johnson K L, Kendall K and Roberts A D 1971 Surface energy and contact of elastic solids *Proc. R. Soc. Lon. Ser.-A* **324** 301
- [31] Jensen K E, Style R W, Xu Q and Dufresne E R 2017 Strain-dependent solid surface stress and the stiffness of soft contacts *Phys. Rev. X* **7** 041031
- [32] Lombardi M L, Knecht D A, Dembo M and Lee J 2007 Traction force microscopy in Dictyostelium reveals distinct roles for myosin II motor and actin-crosslinking activity in polarized cell movement *J. Cell Sci.* **120** 1624–34